HHS Public Access

Author manuscript

ACS Sens. Author manuscript; available in PMC 2022 November 26.

Published in final edited form as:

ACS Sens. 2021 November 26; 6(11): 3967–3977. doi:10.1021/acssensors.1c01225.

Co-polarized [1-^{13}C]pyruvate and [1,3-$^{13}C_2$]acetoacetate Provide a Simultaneous View of Cytosolic and Mitochondrial Redox in a Single Experiment

Gaurav Sharma[1], **Xiaodong Wen**[1], **Nesmine R. Maptue**[1], **Thomas Hever**[1], **Craig R. Malloy**[1,2,3], **A. Dean Sherry**[1,3,4], **Chalermchai Khemtong**[1,3,5,6,*]

[1]Advanced Imaging Research Center, University of Texas Southwestern Medical Center, Dallas, TX, 75390, United States

[2]Department of Internal Medicine, University of Texas Southwestern Medical Center, Dallas, TX, 75390, United States

[3]Department of Radiology, University of Texas Southwestern Medical Center, Dallas, TX, 75390, United States

[4]Department of Chemistry, University of Texas at Dallas, Richardson, TX, 75080, United States.

[5]Department of Medicine, Division of Endocrinology, Diabetes and Metabolism, University of Florida, Gainesville, FL, 32610, United States

[6]Department of Biochemistry and Molecular Biology, University of Florida, Gainesville, FL, 32610, United States

Abstract

Cellular redox is intricately linked to energy production and normal cell function. Although the redox state of mitochondria and cytosol are connected by shuttle mechanisms, the redox state of mitochondria may differ from redox in the cytosol in response to stress. However, detecting these differences in functioning tissue is difficult. Here, we employed ^{13}C magnetic resonance spectroscopy (MRS) and co-polarized [1-^{13}C]pyruvate and [1,3-$^{13}C_2$]acetoacetate ([1,3-$^{13}C_2$]AcAc) to monitor production of hyperpolarized (HP) lactate and β-hydroxybutyrate as indicators of cytosolic and mitochondrial redox, respectively. Isolated rat hearts were examined under normoxic conditions, during low-flow ischemia, and after pretreatment with either aminooxyacetate (AOA) or rotenone. All interventions were associated with an increase in [Pi]/[ATP] measured by ^{31}P NMR. In well-oxygenated untreated hearts, rapid conversion of HP [1-^{13}C]pyruvate to [1-^{13}C]lactate and [1,3-$^{13}C_2$]AcAc to [1,3-$^{13}C_2$]β-hydroxybutyrate

[*]**CORRESPONDING AUTHOR** Chalermchai Khemtong, Department of Medicine, Division of Endocrinology, Diabetes and Metabolism, University of Florida, Gainesville, FL, USA. Phone: +1 (352) 273-8646; chalermchai.khemtong@medicine.ufl.edu.

ASSOCIATED CONTENT

Supporting Information

Supporting Information Available: The following files are available free of charge.

se-2021–01225z.R1_Sharma_SupportingInfo.pdf: Normalized ^{13}C signals of HP [1-^{13}C]lactate, C-1 of HP [1,3-$^{13}C_2$]β-hydroxybutyrate, HP [1-^{13}C]alanine, and HP [1-^{13}C]acetyl-carnitine; and fractional ^{13}C enrichment of total lactate and β-hydroxybutyrate in perfused rat hearts

CONFLICT OF INTEREST

The authors have no conflicts to declare.

([1,3-$^{13}C_2$]β-HB) was readily detected. A significant increase in HP [1,3-$^{13}C_2$]β-HB but not [1-^{13}C]lactate was observed in rotenone-treated and ischemic hearts, consistent with an increase in mitochondrial NADH but not cytosolic NADH. AOA treatments did not alter the productions of HP [1-^{13}C]lactate or [1,3-$^{13}C_2$]β-HB. This study demonstrates that biomarkers of mitochondrial and cytosolic redox may be detected simultaneously in functioning tissue using co-polarized [1-^{13}C]pyruvate and [1,3-$^{13}C_2$]AcAc and ^{13}C MRS, and that changes in mitochondrial redox may precede changes in cytosolic redox.

Graphical Abstract

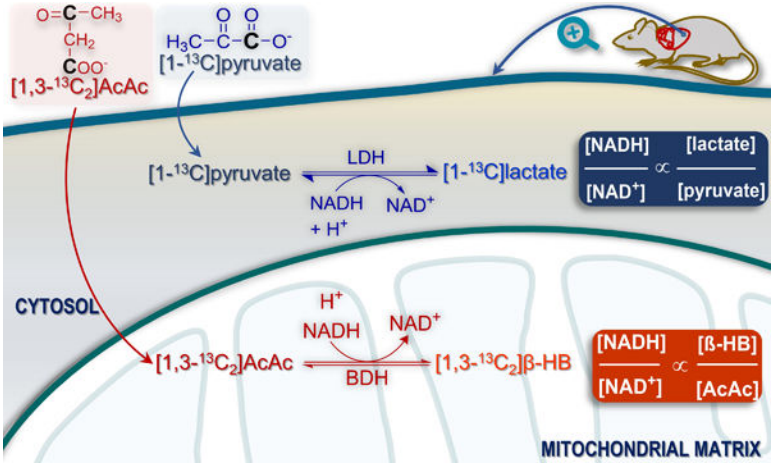

Keywords

redox metabolism; cardiac ischemia; acetoacetate; pyruvate; hyperpolarized ^{13}C MR

The redox state of mitochondria and cytosol plays a critical role in normal cellular bioenergetics, and redox influences other functions such as differentiation, proliferation, and apoptosis. Not surprisingly, abnormal redox homeostasis is linked with many diseases including cancer[1], diabetes[2], heart failure[3], and neurodegenerative disorders[4]. Specific interventions targeting redox such as administration of nicotinamide riboside have been proposed[5]. For the purposes of describing cell energetics, the most important redox pair is NAD^+ and NADH because they serve as co-factors in numerous reactions in compartmentalized pathways such as glycolysis and the TCA cycle. Since the inner mitochondrial membrane is impermeable[3] to pyridine nucleotides, the redox state of the cytosol and mitochondria are linked by two shuttle systems, the malate-aspartate shuttle and the glycerol-3-phosphate shuttle. Although the NAD^+/NADH ratio in these compartments are interconnected, they are not necessarily the same. For example, the ratio of NAD^+ to NADH in skeletal muscle is very high in cytosol (~540) and much lower (~6.3) in mitochondria[6].

Determining redox in functioning tissues is challenging. Destructive biochemical assays measure the combined free and enzyme-bound content of NAD^+ and NADH[7, 8]. The ratio of NAD^+ to NADH, predominantly in mitochondria because of the high NADH content, has

been calculated using fluorescence methods[9], and ^{31}P NMR methods have been proposed [10, 11]. NAD^+ and NADH concentrations have also been measured using genetically encoded fluorescent probes [12, 13]. An approach termed the metabolite indicator method allows for an estimation of the "free" concentration ratio, NAD^+/NADH, by measuring concentrations of cellular redox pairs, typically lactate and pyruvate in the cytosol, and β-hydroxybutyrate and acetoacetate in the mitochondria [14–16]. This method rests on the assumption that the substrates and products of these reactions are in rapid exchange and near equilibrium.

Hyperpolarization (HP) methods have been introduced recently to monitor metabolism of ^{13}C-labeled pyruvate or other small molecules involved with redox reactions. Multiple earlier studies have emphasized the potential applications of HP for monitoring redox, for example by monitoring the redox pair, [1-^{13}C]ascorbic acid and [1-^{13}C]dehydroascorbic acid [17–19]. Ketones have attracted considerable attention because of their intimate involvement with redox reactions and also because they are readily oxidized in many tissues. Others have also demonstrated that more than one compound may be polarized and injected simultaneously, with independent detection of metabolic products because of the chemical shift [20–23].

The goal of this study was to explore the combination of hyperpolarized (HP) [1-^{13}C]pyruvate and [1,3-$^{13}C_2$]acetoacetate ([1,3-$^{13}C_2$]AcAc) to probe mitochondrial and cytosolic redox simultaneously in the isolated heart. The heart was chosen because redox control has been extensively investigated [24–26], and HP exams with pyruvate during pharmacologic stress are feasible[27, 28]. The effects of interventions known to interfere with normal redox control (low-flow ischemia or rotenone, a complex I inhibitor) or function of the malate-aspartate shuttle (aminooxyacetate, AOA) were evaluated. All interventions were associated with a decrease in oxygen consumption and a decrease in [phosphocreatine]/[ATP] measured by ^{31}P NMR spectroscopy, demonstrating significant disruption of normal energetics. The ratio HP [1,3-$^{13}C_2$]β-hydroxybutyrate/[1-^{13}C]acetyl carnitine was sensitive to both low-flow ischemia and rotenone. In contrast, the HP [1-^{13}C]lactate/[1-^{13}C]alanine was not significantly altered, although the trends were similar. These results suggest that mitochondrial redox is a more sensitive indicator of redox stress in the tissue, at least with these interventions. Metabolism of co-polarized [1,3-$^{13}C_2$]AcAc and [1-^{13}C]pyruvate provides a new approach to detecting altered redox state in distinct intracellular compartments of functioning tissues.

RESULTS

Physiological measurements

Hearts were supplied with a mixture of glucose, pyruvate, lactate, and long-chain fatty acids at physiological concentrations and fully oxygenated conditions for 20 minutes, then exposed to low perfusion pressure, 20 μM rotenone, or 0.1 mM AOA, followed by collection of a single ^{31}P spectrum. Co-polarized [1-^{13}C]pyruvate and [1,3-$^{13}C_2$]AcAc was then injected and dynamic ^{13}C NMR spectra were collected. Each heart was then immediately freeze-clamped for further analysis. The time line for this experiment is summarized in Fig. 1A and a schematic of the major metabolic reactions involved is shown in Fig. 1B. During the initial 20 minutes of normoxic perfusion, myocardial oxygen consumption (MVO_2) and

heart rates were similar in all hearts. The measured coronary flows were 16.6 ± 1.4, 6.2 ± 1.5, 22.8 ± 0.8, and 23.0± 1.2 mL/min for control, low-flow ischemia, rotenone-treated, and AOA-treated hearts, respectively (Fig. 2A). Oxygen consumption measured at the same time point of the control hearts was 16.6 ± 1.1 μmol/min/g d.w. Lower oxygen consumption values were observed in all three treatment groups (6.4 ± 1.5, 6.1 ± 0.7, and 8.3 ± 0.8 μmol/min/g d.w. for low-flow ischemia, rotenone and AOA respectively, Fig. 2B). The intracellular pH as measured by ^{31}P NMR decreased from 7.18 ± 0.01 (normoxia) to 6.97 ± 0.02 (low-flow ischemia), 6.94 ± 0.02 (rotenone), and 6.97 ± 0.01 (AOA) (Fig. 2C). A marked decrease (80%) in the phosphocreatine to ATP ratio ([PCr]/[ATP]) and, correspondingly, a large increase (221%) in the inorganic phosphate to ATP ratio ([P_i]/[ATP]) were observed in rotenone-treated hearts as compared with the control group (Figs. 3A–B). These ratios in the hearts treated with AOA and low-flow ischemia are not statistically different from the control group. The concentration of ADP ([ADP], Fig. 3C) was estimated from the ^{31}P NMR results using methods previously described by Clarke et al.[29]. A significant increase (6.8-fold) in [ADP] was observed in rotenone-treated hearts (1.25 ± 0.29 mM) over the control hearts (0.18 ± 0.06 mM). The concentration of this metabolite in low-flow ischemic (0.22 ± 0.03 mM) and AOA-treated (0.34 ± 0.07 mM) hearts was not statistically different from the baseline group. The calculated phosphorylation potentials ([ATP]/[ADP]·[Pi])[29] were 12.99 ± 3.60, 6.44 ± 1.74, 0.52 ± 0.12, 3.04 ± 0.76 mM^{-1} for control, low-flow ischemic, rotenone-treated, and AOA-treated hearts, respectively. The results show a significant decrease in phosphorylation potential as a result of rotenone and AOA treatments (Fig. 3D) but the low-flow ischemic group did not differ statistically from the control group.

Metabolism of hyperpolarized [1-^{13}C]pyruvate and [1,3-$^{13}C_2$]AcAc

A representative stacked plot and corresponding summed spectrum with peak assignments are shown in Figures 4A and 4B. Representative stacked plots of time-resolved ^{13}C spectra in Fig. 4C show the evolution of metabolic products of [1-^{13}C]pyruvate, designated as P1-P4, and [1,3-$^{13}C_2$]AcAc, designated as A1-A4. The corresponding summed spectrum from 40 consecutive acquisitions are shown in Fig. 4D. In all four spectra, resonances of downstream metabolites derived from HP [1-^{13}C]pyruvate and HP [1,3-$^{13}C_2$]AcAc are clearly detectable. The metabolism of HP [1-^{13}C]pyruvate yielded a small HP ^{13}C-bicarbonate signal (160.9 ppm), [1-^{13}C]alanine (176.5 ppm), and [1-^{13}C]lactate (183.2 ppm). HP [1,3-$^{13}C_2$]AcAc yielded HP [1,3-$^{13}C_2$]β-HB with peaks resonating at 180.6 ppm (C1) and 66.5 ppm (C3, doublet, J_{CH} = 141.4 Hz), and [1-^{13}C]acetyl-carnitine (173.9 ppm). It is important to point out that the peak appearing at 181.6 ppm is likely an overlapped peak of HP [1-^{13}C]acetate and HP [5-^{13}C]glutamate. [1-^{13}C]Acetate could be generated nonenzymatically as a byproduct during the hydrolysis of ethyl [1,3-$^{13}C_2$]acetoacetate. [5-^{13}C]Glutamate was produced via oxidative metabolism of [1,3-$^{13}C_2$]AcAc and [1-^{13}C]acetate. The peak at 179.0 ppm was assigned to pyruvate hydrate. At each time point, the signal intensity of HP [1-^{13}C]lactate was normalized to the total signal of all downstream metabolites originated from HP [1-^{13}C]pyruvate, i.e. [1-^{13}C]alanine, [1-^{13}C]lactate, and ^{13}C-bicarbonate summed over the NMR acquisition time window for each heart. Similarly, the signal intensity of C-1 of [1,3-$^{13}C_2$]β-HB was normalized to the total signals of [1-^{13}C]acetyl-carnitine and C-1 of [1,3-$^{13}C_2$]β-HB over

the same period. The average normalized intensities (4 hearts per group) versus perfusion time for all four groups are shown in Fig. 4E and Fig. 4F. For all four groups, the normalized intensities from [1-^{13}C]lactate (Fig.S1A), [1-^{13}C]alanine (Fig.S1B), [1,3-$^{13}C_2$]β-HB (Fig.S1C) and [1-^{13}C]acetyl-carnitine (Fig.S1D) are shown. As bicarbonate is produced by spontaneous decarboxylation of acetoacetate in addition to metabolism, it was omitted from the analysis.

The signals from [1-^{13}C]lactate tend to be higher in all three treatment groups but did not reach statistical significance compared to control. However, the signal of HP [1,3-$^{13}C_2$]β-HB was higher in rotenone and low-flow ischemic hearts compared to controls. Similar trends were also observed when comparing the ratios of HP [1-^{13}C]lactate/[1-^{13}C]alanine (Fig. 5A) and HP [1,3-$^{13}C_2$]β-HB/[1-^{13}C]acetyl-carnitine (Fig. 5B). Again, no significant differences were detected in the [1-^{13}C]lactate/[1-^{13}C]alanine ratios among the four groups while the [1,3-$^{13}C_2$]β-HB/[1-^{13}C]acetyl-carnitine ratios did increase significantly in the low flow ischemia hearts (3-fold higher) and rotenone-treated group (~2.6-fold higher). This ratio also tended to be higher in hearts treated with AOA but differences between control hearts did not reach statistical significance. Caution must be exercised, however, when using [1-^{13}C]lactate/[1-^{13}C]alanine and [1,3-$^{13}C_2$]β-HB/[1-^{13}C]acetyl-carnitine ratios as metrics for cytosolic and mitochondrial redox. Alanine transaminase participates in shuttling NADH between the cytosol and mitochondria, and oxidation of acetoacetate involves CoA which is critical in regulating PDH flux, which in turn is redox sensitive. Despite the apparent link to cellular redox, productions of HP [1-^{13}C]alanine and [1-^{13}C]acetyl-carnitine from the injected probes do not involve hydride transfer and therefore are not expected to be highly sensitive to redox changes. While it is likely that signals of HP [1-^{13}C]alanine and [1-^{13}C]acetyl-carnitine may vary slightly under different perfusion conditions, metabolite signal ratios obtained by normalizing HP [1-^{13}C]lactate and [1,3-$^{13}C_2$]β-HB signals to [1-^{13}C]alanine and [1-^{13}C]acetyl-carnitine, respectively, may present as an alternative metric for assessing changes in cytosolic and mitochondrial redox.

Myocardial lactate and β-hydroxybutyrate concentrations in freeze-clamped tissue

All hearts were removed from the NMR system and freeze-clamped immediately after the ^{13}C NMR acquisition had ended (about 8 min after HP injection). Hearts were subsequently extracted with perchloric acid, neutralized, freeze-dried, and redissolved in D_2O for analysis by high-resolution ^{1}H NMR. The methyl proton resonances of lactate and β-HB each appear as doublets due to 3-bond J_{HH} coupling surrounded by smaller satellite peaks reflecting J_{CH} couplings arising from [1-^{13}C]lactate and [1,3-$^{13}C_2$]β-HB contributions to these metabolite pools (Fig. 6A and 6B). The concentrations of these metabolites were estimated from peak intensities, calculated from areas under the resonances, of the methyl resonance of lactate or β-HB and the reference resonance of DSS (at 0 ppm) using a predetermined calibration curve. The tissue concentrations in micromoles per gram dry weight (μmol/g d.w.) are reported in Fig. 6C–6F. Hearts treated with AOA had the highest concentration of [1-^{13}C]lactate produced from HP [1-^{13}C]pyruvate (2.18 ± 0.50 μmol/g d.w., Fig. 6B). The other groups had similar concentrations of [1-^{13}C]lactate: control (1.28 ± 0.19 μmol/g d.w.), low-flow ischemia (1.60 ± 0.22 μmol/g d.w), and rotenone-treated hearts (1.36 ± 0.41 μmol/g d.w.). Interestingly, only a small fraction of the total lactate pool, 4 to 6% in all

groups (Fig. 6E) was ^{13}C labeled as indicated by the total lactate concentrations in heart extracts (control: 30 ± 3 μmol/g d.w., low flow ischemia: 22 ± 3 μmol/g d.w., rotenone treated: 19 ± 2 μmol/g d.w. and AOA treated: 42 ± 6 μmol/g d.w.).

Higher concentrations of ^{13}C-labelled β-HB enzymatically converted from ^{13}C-labelled acetoacetate were observed in all three study groups compared to the values measured in control hearts. The concentrations of this metabolite were 0.03 ± 0.01, 0.27 ± 0.01, 0.12 ± 0.04, and 0.14 ± 0.04 μmol/g d.w. for control hearts, low-flow ischemic hearts, rotenone-treated hearts, and AOA-treated hearts, respectively. These results show that low-flow ischemia hearts produced the highest concentration of ^{13}C-labeled β-HB, a 9-fold increase over the control hearts (Fig. 6D). Rotenone and AOA treatment also resulted in increased ^{13}C-labelled β-HB production, albeit to a smaller extent, compared to the control group. Interestingly, total tissue β-HB (^{13}C-labelled plus endogenous β-HB) concentrations in these hearts show a different trend (Fig. 6F). The highest total β-HB concentration was observed in the AOA-treated hearts (1.17 ± 0.28 μmol/g d.w.). Despite having the highest ^{13}C-labeled β-HB concentration, the average total β-HB concentration in low-flow ischemia hearts (0.40 ± 0.06 μmol/g d.w.) is slightly higher than the control group (0.25 ± 0.20 μmol/g d.w.). Total β-HB concentration in the rotenone-treated group was 0.60±0.17 μmol/g d.w.

DISCUSSION

The goal of this study was to investigate whether co-hyperpolarized [1-^{13}C]pyruvate and [1,3-$^{13}C_2$]AcAc might be useful for simultaneous detection of redox state in the cytosolic and mitochondria compartments in a single exam. Imaging cellular metabolism with hyperpolarized [1-^{13}C]pyruvate has been extensively studied preclinically[30–33] and is beginning to be used in clinical trials.[34–37] The appearance of hyperpolarized ^{13}C-bicarbonate is widely accepted as a biomarker of oxidative metabolism while the appearance of hyperpolarized [1-^{13}C]lactate is thought to reflect a variety of indices including lactate pool size, LDH activity, and cytosolic redox.[27, 38–40] Hyperpolarized [1-^{13}C]AcAc has also been tested in preclinical models for monitoring ketone body utilization[41–45] and conversion of [1,3-^{13}C]AcAc to [1,3-^{13}C] β-HB has been used as an index of mitochondrial redox state in isolated perfused rat hearts and rat kidneys in vivo[43, 45]. These earlier concepts were combined in the present study by co-polarizing these two ^{13}C metabolic probes to evaluate their effectiveness as indicators of cytosolic and mitochondrial redox in isolated perfused rat hearts experiencing a variety of physiological stresses.

Low-flow ischemia induced by lowering the perfusion pressure resulted in reduced oxygen consumption, intracellular acidification, and NADH accumulation, consistent with our previous findings.[43] Increased production of [1,3-$^{13}C_2$]β-HB was observed in these ischemic hearts, consistent with higher levels of mitochondrial NADH reported in hearts subjected to similar ischemic conditions.[43, 46, 47] Interestingly, although the [PCr]/[ATP] and phosphorylation potential measured in ischemic hearts tended to be lower compared to control, they were not statistically different from the control hearts. In contrast, the amount of HP [1,3-$^{13}C_2$]β-HB produced from [1,3-$^{13}C_2$]AcAc was significantly higher in ischemic hearts compared to control hearts. Our findings suggest that mitochondrial dysfunction in hearts subjected to mild ischemia is more readily detected by HP ^{13}C NMR than by ^{31}P

NMR. Our results also suggest that the metabolism of HP[1,3-$^{13}C_2$]AcAc to [1,3-$^{13}C_2$]β-HB is a more sensitive index for mitochondrial redox changes induced by myocardial ischemia than traditional methods of measuring tissue and arterial β-HB/AcAc ratios as an index for mitochondrial redox in the heart. Specifically, Opie *et al.* reported that the ketone body ratios in isolated perfused rat hearts[48] and heart biopsies from dogs subjected to coronary arterial ligation[49] could not be reliably measured due to low ketone body concentrations in these tissues. Both studies also reported that ratios of extracellular β-HB and AcAc are not indicative of the mitochondrial redox in the hearts.

Rotenone, an inhibitor of mitochondrial complex I, does not have its primary effect on myocardial perfusion, unlike low-flow ischemia as illustrated in Figure 2. With a significant increase in coronary flow, rotenone treatment was associated with reduced oxygen consumption, intracellular acidification, and significantly reduced phosphorylation potential reflecting impaired respiration. Hearts treated with rotenone produced significantly more [1,3-$^{13}C_2$]β-HB than control hearts, consistent with increased mitochondrial NADH.[43, 47, 50, 51]

Inhibition of the malate-aspartate shuttle with AOA would be expected to increase cytosolic retention of NADH while decreasing mitochondrial NADH availability, although the effects of AOA on cardiac redox have not been studied.[52–54] As with rotenone, coronary flow was preserved or slightly increased. Although reduced oxygen consumption, intracellular acidification, and decreased phosphorylation potential was observed, accumulation of P_i was not high. A [PCr]/[ATP] ratio comparable to that in control hearts suggests that mitochondrial function is not greatly affected by AOA. These findings are consistent with the HP ^{13}C NMR results where no change in HP [1,3-$^{13}C_2$]β-HB production was observed in AOA-treated hearts.

Somewhat unexpectedly, no statistically significant differences in the production of HP [1-^{13}C]lactate were found across the four groups of hearts. These interventions were chosen because of known effects on cytosolic redox state in hearts. For example, cytosolic redox state in low-flow ischemic hearts was highly altered as confirmed by a marked increase in tissue lactate-to-pyruvate ratio.[55, 56] Similarly, rotenone treatments resulted in elevated lactate[57] and NADH[58] levels in myocytes. AOA treatments increased the lactate-to-pyruvate and NADH/NAD^+ ratios in isolated working hearts and smooth muscle cells[52, 53, 59] Although there was a trend to increase lactate in the HP exams, the effects of these interventions were not dramatic. The similar HP [1-^{13}C]lactate signals across four groups of hearts may be due to a combination of factors. Since these hearts were supplied with exogenous lactate and pyruvate in physiological concentrations with continuous flow throughout, the preexisting pool of endogenous lactate were high in all four groups of hearts (~20–40 μmol/g d.w., Fig. 6E). Upon entering the cells, HP [1-^{13}C]pyruvate rapidly exchanges into a large, constant pool size of unlabeled lactate producing a large, constant amount of HP [1-^{13}C]lactate. This exchange has been shown to occur with little, if any, net production of new lactate.[60, 61] The small and comparable ^{13}C-lactate fractional enrichments (4–8%, Fig. S2) across the groups of hearts agree well with the real-time HP ^{13}C NMR results, consistent with exchange of HP [1-^{13}C]pyruvate into preexisting lactate pools.

In contrast, the ^{1}H NMR spectra showed varying degrees of ^{13}C-labeling (11–73% ^{13}C fractional enrichment) in the β-HB pool at the time of freeze-clamping (Figures 6B and S2). The largest preexisting β-HB pool was observed in the AOA-treated hearts. However, the ^{13}C fractional enrichment in this group is not statistically different from that of the control hearts, consistent with the HP ^{13}C results. This finding, in marked contrast to the observations of lactate, indicate that the products of [1,3-$^{13}C_2$]AcAc are not necessarily affected by the preexisting ketone pool in the myocardium. This feature may play a role in the sensitivity of [1,3-$^{13}C_2$]β-HB to stress. Another factor is that the mass of NADH available in mitochondria and the cytosol in functioning hearts is quite different. Using simple assumptions about mitochondrial volume and measured NAD^+ and NADH in both compartments [13, 62, 63] the mass of NADH in normal mitochondria, 0.06 micromoles/gram dry weight, is 10 to 100 times higher than the NADH available in the cytosol. Hence, the pool of available NADH in mitochondria may enable a rapid reduction of acetoacetate.

In principle, clinical translations of this technology could allow for the myocardial redox state to be assessed in a single HP ^{13}C MRI exam by measuring HP [1,3-$^{13}C_2$]β-HB and [1-^{13}C]lactate in the heart, but at least three other factors should be considered. First, chemical dispersions between crucial metabolites, [1-^{13}C]lactate, C-1 of [1,3-$^{13}C_2$]β-HB, and byproduct [1-^{13}C]acetate, are somewhat small (~1 ppm), potentially making it challenging to resolve these metabolite peaks. However, a recent in vivo HP ^{13}C MRI study found that it is possible to resolve [1-$_{13}$C]β-HB from [1-^{13}C]acetate in rat kidneys using a clinical 3T MRI scanner.[45] Second, the two probes may compete with one another for the same cellular transport system. Pyruvate and acetoacetate are transported by the same monocarboxylate transporter (MCT) systems.[64] The K_m for pyruvate transport in some cells is about 2 mM but is much lower in oocytes.[65] The K_m for acetoacetate ranges from 0.8 mM to over 200 mM depending on the isoform.[64] More recently, the importance of MCT-1 in the rate-limited appearance of lactate in an HP exam was clearly demonstrated.[66] The magnitude of the interaction may differ among tissues since the MCT isoforms may differ. Finally, the effect of injected probes on cellular redox must be considered. Both substrates are part of the major mitochondrial and cytosolic redox pairs. Equilibration of pyruvate with lactate and acetoacetate with β-HB will consume NADH in their respective compartments. Nevertheless, both pyruvate and acetoacetate are rapidly oxidized to acetyl-CoA, replenishing NADH. Therefore, administrations of these substrates over a brief period could momentarily influence redox.

In summary, co-polarized [1,3-$^{13}C_2$]AcAc and [1-^{13}C]pyruvate allow detection of the redox response in cytosol and mitochondria of the isolated heart. Although there are challenges to clinical translation, this combination could potentially be used as a biomarker for altered redox state in distinct intracellular compartments of tissues.

METHODS

Animals and heart perfusion

Animal studies were approved by the Institutional Animal Care and Use Committee (IACUC) at UT Southwestern Medical Center. Metabolism of co-hyperpolarized [1-^{13}C]pyruvate and [1,3-$^{13}C_2$]AcAc were investigated in Sprague Dawley rats in four

groups (n = 4 per group), control hearts (Control), low-flow ischemic hearts (LF Isch.), hearts treated with a mitochondrial complex I inhibitor rotenone (Rotenone), and hearts treated with a transaminase inhibitor aminooxyacetate (AOA). Hearts were excised and retrogradely perfused according to the Langendorff method as previously described[43]. The phosphate-free modified Krebs-Henseleit (KH) perfusion solution (25 mM $NaHCO_3$, 118 mM NaCl, 4.7 mM KCl, 1.2 mM $MgSO_4$, 1.2 mM KH_2PO_4 and 1.25 mM $CaCl_2$) contained a physiological mixture of glucose (5.5 mM), lactate (1.2 mM), pyruvate (0.12 mM), and long-chain free fatty acids (0.4 mM) in bovine serum albumin (0.75%). The free fatty acids were a mixture of palmitic acid (23.7 mole %), palmitoleic acid (5.6 mole %), stearic acid (2.6 mole %), oleic acid (26.3 mole %), linoleic acid (37.0 mole %), γ-linoleic acid (2.4 mole %), and docosahexaenoic acid (2.3 mole %). The perfusion solution was oxygenated with a 95:5 mixture of O_2/CO_2 at a constant pressure of 100 cm-H_2O. After 20 min of perfusion, the perfusion pressure was lowered to 25-cm H_2O for the low-flow ischemia group. At this time point, the rotenone and AOA hearts were exposed to rotenone (20 μM) or AOA (100 μM), respectively. Shimming was performed using the ^{23}Na-FID to a linewidth of ~14 Hz while the heart was surrounded by a sucrose flush (250 mM) to remove extracellular ^{23}Na. The NMR probe was then tuned to ^{31}P without altering myocardial perfusion or shimming followed by ^{31}P NMR acquisition of the perfused hearts using 90-deg pulses (number of transients = 64). ^{31}P Chemical shifts were referenced to the phosphocreatine (PCr) resonance set to 0 ppm. The intracellular pH of these hearts was measured from the chemical shift of the inorganic phosphate (Pi) peak using a modified Henderson–Hasselbalch equation, $pH = 6.72 + \log[(\delta_{Pi}-3.17)/(5.72-\delta_{Pi})]$, as described previously[43, 67]. Concentration ratios of PCr, Pi, and ATP were measured using ^{31}P signal intensities of each metabolite (γ-phosphate for ATP). The ratios for [Pi]/[ATP] and [PCr]/[ATP] were corrected for T1-induced signal intensity differences using the equation described previously by Bottomley *et al.*[68] based on the T_1 values reported by Spencer *et al.*[69] for PCr, Pi, and ATP. The ADP concentration (Eq. 1) and phosphorylation potential (Eq. 2) were calculated as reported by Clarke et al. using the T_1 corrected ratios for [Pi]/[ATP] and [PCr]/[ATP], proton concentrations calculated from pH values (Fig. 2C) and reported values for creatine kinase equilibrium constant ($K_{CK} = 10^9$/[mol]), total creatine concentration (28.3 mmol/L) and total ATP concentration (6.27 mmol/L)[29].

$$[ADP] = \frac{[ATP][Cr]}{[PCr][H^+]K_{CK}} \quad \text{Eq. 1}$$

$$\frac{[ATP]}{[ADP][Pi]} = \frac{[PCr][H^+]K_{CK}}{[Cr][Pi]} \quad \text{Eq. 2}$$

The coronary flow (CF), developed pressure, heart rate (HR), and oxygen partial pressure (pO_2) were measured twice at ~20 min (baseline) and ~45 min (steady-state). A solution of HP ^{13}C-pyruvate and ^{13}C-acetoacetate was injected into the perfused heart ~30 min of ischemia, rotenone-, or AOA-treatment immediately followed by dynamic ^{13}C NMR. No changes to the perfusion protocol were made for the control hearts during this treatment or ischemia period. In total, each heart was perfused for ~50 min before being freeze clamped.

Polarization and dissolution of [1-^{13}C]pyruvate and [1,3-$^{13}C_2$]AcAc

Solutions of [1-^{13}C]pyruvate (Cambridge Isotope Laboratories, MA, USA) and [1,3-^{13}C]AcAc (Cambridge Isotope Laboratories, MA, USA) were prepared separately for polarization as previously described[32, 43]. Briefly, neat [1-^{13}C]pyruvate was mixed with OX063 (15 mM) and gadoteridol ([Gd^{3+}] = 2 mM)[32]. A [1,3-$^{13}C_2$]AcAc solution, prepared by hydrolysis of ethyl [1,3-$^{13}C_2$]AcAc with 5 M NaOH at 45 °C for 45 min, was mixed with an equal volume of glycerol and added OX063 (15 mM) and gadoteridol ([Gd^{3+}] = 2mM)[43]. To be polarized, the ^{13}C-pyruvate (4 μL) and ^{13}C-acetoacetate (36 μL) solutions were sequentially added into a polarization sample cup placed in liquid nitrogen forming separate layers of the ^{13}C-enriched substrates. The frozen solutions were then loaded into a 3.35T HyperSense polarizer (Oxford Instruments, UK) and polarized for 2 h at ~1.4 K with ~94.1 GHz microwave irradiation. The polarized sample was quickly dissolved in the superheated KH buffer (4 mL). Three milliliters of the co-polarized solution was mixed with additional KH buffer (20 mL) and injected directly into the perfused heart through a polyethylene catheter. Final concentrations for both ^{13}C-pyruvate and ^{13}C-acetoacetate injected into the heart were 2 mM.

^{13}C NMR spectroscopy

After acquisition of ^{31}P NMR data, the probe was rapidly retuned without altering myocardial perfusion or shimming. ^{13}C NMR acquisition was initiated concurrently with the start of the injection of HP substrates. A series of ^{13}C NMR spectra were collected with a 2 s delay between each scan using 20-deg pulses in a 9.4 T (Varian INOVA) spectrometer equipped with a 25-mm broadband probe (Doty Scientific). The hearts were freeze-clamped quickly after the ^{13}C NMR acquisition. NMR spectra were processed using ACD Labs SpecManager (Advanced Chemistry Development, Inc., Canada). Peak areas for each metabolite were normalized to the total ^{13}C signals from the respective injected ^{13}C substrate. Stacked hyperpolarized ^{13}C NMR spectra of the perfused hearts were generated using custom MATLAB scripts (MATLAB R2018a; The MathWorks Inc, USA).

High-resolution NMR spectroscopy of tissue extracts

Frozen heart tissues were pulverized and extracted with 5% perchloric acid (v/v). The extracts were then neutralized, freeze-dried, and reconstituted in D_2O containing 1 mM EDTA and 0.5 mM 2,2-dimethyl-2-silapentane-5-sulfonate (DSS, Chenomx Inc., Canada) as an internal chemical shift reference. High-resolution NMR spectra were acquired on a 14.1 T spectrometer equipped with a 10-mm Bruker cryoprobe. The FID's were zero-filled to 64k data points, Fourier-transformed, referenced to DSS, phased and baseline corrected using ACD/NMR Processor. Tissue concentrations of lactate and β-hydroxybutyrate were estimated using the Chenomx software).

Statistical analysis

Data were presented as mean ± standard error of mean (SEM). All plots were generated using GraphPad Prism v.9 (GraphPad Software, San Diego, USA). Statistical significances of differences were evaluated using a two-tailed Student's t-test with Welch's correction and indicated by $p < 0.05$ (*$p < 0.05$, **$p < 0.01$, ***$p < 0.001$).

Supplementary Material

Refer to Web version on PubMed Central for supplementary material.

ACKNOWLEDGEMENTS

We thank the following agencies for financial support: National Institutes of Health (R37HL034557, P41EB015908, R01EB027698), American Heart Association (18POST34050049), Department of Cardiovascular and Thoracic Surgery at UT Southwestern Medical Center (G.S.).

ABBREVIATIONS

β-HB	β-hydroxybutyrate
β-HBDH	β-hydroxybutyrate dehydrogenase
AcAc	acetoacetate
AOA	aminooxyacetate
ATP	adenosine triphosphate
AUC	area under the curve
HP	hyperpolarized
^{13}C MRS	carbon-13 magnetic resonance spectroscopy
^{13}C MRI	carbon-13 magnetic resonance imaging
DNP	dynamic nuclear polarization
DSS	2,2-dimethyl-2-silapentane-5-sulfonate
[Gd^{3+}]	Gadolinium (III)
KH	Krebs Henseleit
LF	ischemia low-flow ischemia
MVO_2	myocardial oxygen consumption
NAD^+	nicotinamide adenine dinucleotide
NADH	nicotinamide adenine dinucleotide
NMR	nuclear Magnetic Resonance
PCr	phosphocreatine
P_i	inorganic phosphate
Rot	rotenone

REFERENCES

1. Wang K; Jiang J; Lei Y; Zhou S; Wei Y; Huang C, Targeting Metabolic–Redox Circuits for Cancer Therapy. Trends in Biochemical Sciences 2019, 44 (5), 401–414. [PubMed: 30679131]
2. Watson JD, Type 2 diabetes as a redox disease. The Lancet 2014, 383 (9919), 841–843.
3. Berthiaume JM; Kurdys JG; Muntean DM; Rosca MG, Mitochondrial NAD+/NADH Redox State and Diabetic Cardiomyopathy. Antioxidants & Redox Signaling 2017, 30 (3), 375–398. [PubMed: 29073779]
4. Chen Y-Y; Wang M-C; Wang Y-N; Hu H-H; Liu Q-Q; Liu H-J; Zhao Y-Y, Redox signaling and Alzheimer's disease: from pathomechanism insights to biomarker discovery and therapy strategy. Biomarker Research 2020, 8 (1), 42. [PubMed: 32944245]
5. Diguet N; Trammell Samuel AJ; Tannous C; Deloux R; Piquereau J; Mougenot N; Gouge A; Gressette M; Manoury B; Blanc J; Breton M; Decaux J-F; Lavery Gareth G; Baczkó I; Zoll J; Garnier A; Li Z; Brenner C; Mericskay M, Nicotinamide Riboside Preserves Cardiac Function in a Mouse Model of Dilated Cardiomyopathy. Circulation 2018, 137 (21), 2256–2273. [PubMed: 29217642]
6. Putman CT; Jones NL; Hultman E; Hollidge-Horvat MG; Bonen A; McConachie DR; Heigenhauser GJF, Effects of short-term submaximal training in humans on muscle metabolism in exercise. American Journal of Physiology-Endocrinology and Metabolism 1998, 275 (1), E132–E139.
7. Yang H; Yang T; Baur JA; Perez E; Matsui T; Carmona JJ; Lamming Dudley W.; Souza-Pinto NC; Bohr VA; Rosenzweig A; de Cabo R; Sauve Anthony A.; Sinclair DA, Nutrient-Sensitive Mitochondrial NAD+ Levels Dictate Cell Survival. Cell 2007, 130 (6), 1095–1107. [PubMed: 17889652]
8. Xie W; Xu A; Yeung ES, Determination of NAD+ and NADH in a Single Cell under Hydrogen Peroxide Stress by Capillary Electrophoresis. Analytical Chemistry 2009, 81 (3), 1280–1284. [PubMed: 19178345]
9. Chance B; Cohen P; Jobsis F; Schoener B, Localized Fluorometry of Oxidation-Reduction States of Intracellular Pyridine Nucleotide in Brain and Kidney Cortex of the Anesthetized Rat. Science 1962, 136 (3513), 325.
10. Lu M; Zhu X-H; Zhang Y; Chen W, Intracellular redox state revealed by in vivo 31P MRS measurement of NAD+ and NADH contents in brains. Magnetic Resonance in Medicine 2014, 71 (6), 1959–1972. [PubMed: 23843330]
11. Ren J; Malloy CR; Sherry AD, Quantitative measurement of redox state in human brain by (31) P MRS at 7T with spectral simplification and inclusion of multiple nucleotide sugar components in data analysis. Magn Reson Med 2020, 84 (5), 2338–2351. [PubMed: 32385936]
12. Cambronne XA; Stewart ML; Kim D; Jones-Brunette AM; Morgan RK; Farrens DL; Cohen MS; Goodman RH, Biosensor reveals multiple sources for mitochondrial NAD(+). Science 2016, 352 (6292), 1474–7. [PubMed: 27313049]
13. Zhao Y; Yang Y; Loscalzo J, Real-time assessment of the metabolic profile of living cells with genetically encoded NADH sensors. Methods Enzymol 2014, 542, 349–67. [PubMed: 24862275]
14. Kiuchi T; Ozawa K; Yamamoto Y; Takayasu T; Maki A; Shimahara Y; Mori K; Kobayashi N; Yamaoka Y; Kumada K, Changes in arterial ketone body ratio in the phase immediately after hepatectomy. Prognostic implications. Arch Surg 1990, 125 (5), 655–9. [PubMed: 2331225]
15. Klingenberg M; Buecher T, Biological oxidations. Annu Rev Biochem 1960, 29, 669–708. [PubMed: 14409905]
16. Levy B; Sadoune LO; Gelot AM; Bollaert PE; Nabet P; Larcan A, Evolution of lactate/pyruvate and arterial ketone body ratios in the early course of catecholamine-treated septic shock. Crit Care Med 2000, 28 (1), 114–9. [PubMed: 10667509]
17. Keshari KR; Sai V; Wang ZJ; VanBrocklin HF; Kurhanewicz J; Wilson DM, Hyperpolarized [1-¹³C]Dehydroascorbate MR Spectroscopy in a Murine Model of Prostate Cancer: Comparison with ¹⁸F-FDG PET. Journal of Nuclear Medicine 2013, 54 (6), 922. [PubMed: 23575993]
18. Keshari KR; Wilson DM; Sai V; Bok R; Jen KY; Larson P; Van Criekinge M; Kurhanewicz J; Wang ZJ, Noninvasive in vivo imaging of diabetes-induced renal oxidative stress and response to

therapy using hyperpolarized 13C dehydroascorbate magnetic resonance. Diabetes 2015, 64 (2), 344–52. [PubMed: 25187363]

19. Bohndiek SE; Kettunen MI; Hu D.-e.; Kennedy BWC; Boren J; Gallagher FA; Brindle KM, Hyperpolarized [1–13C]-Ascorbic and Dehydroascorbic Acid: Vitamin C as a Probe for Imaging Redox Status in Vivo. Journal of the American Chemical Society 2011, 133 (30), 11795–11801. [PubMed: 21692446]
20. Lau AZ; Miller JJ; Robson MD; Tyler DJ, Simultaneous assessment of cardiac metabolism and perfusion using copolarized [1–13C]pyruvate and 13C-urea. Magnetic Resonance in Medicine 2017, 77 (1), 151–158. [PubMed: 26743440]
21. von Morze C; Sukumar S; Reed GD; Larson PEZ; Bok RA; Kurhanewicz J; Vigneron DB, Frequency-specific SSFP for hyperpolarized 13C metabolic imaging at 14.1 T. Magnetic Resonance Imaging 2013, 31 (2), 163–170. [PubMed: 22898680]
22. von Morze C; Larson PEZ; Hu S; Yoshihara HAI; Bok RA; Goga A; Ardenkjaer-Larsen JH; Vigneron DB, Investigating tumor perfusion and metabolism using multiple hyperpolarized 13C compounds: HP001, pyruvate and urea. Magnetic Resonance Imaging 2012, 30 (3), 305–311. [PubMed: 22169407]
23. Wilson DM; Keshari KR; Larson PEZ; Chen AP; Hu S; Criekinge MV; Bok R; Nelson SJ; Macdonald JM; Vigneron DB; Kurhanewicz J, Multi-compound polarization by DNP allows simultaneous assessment of multiple enzymatic activities in vivo. Journal of Magnetic Resonance 2010, 205 (1), 141–147. [PubMed: 20478721]
24. Nuutinen EM, Subcellular origin of the surface fluorescence of reduced nicotinamide nucleotides in the isolated perfused rat heart. Basic Res Cardiol 1984, 79 (1), 49–58. [PubMed: 6233965]
25. Steenbergen C; Deleeuw G; Barlow C; Chance B; Williamson JR, Heterogeneity of the hypoxic state in perfused rat heart. Circulation Research 1977, 41 (5), 606–615. [PubMed: 908108]
26. Chance B, Pyridine nucleotide as an indicator of the oxygen requirements for energy-linked functions of mitochondria. Circulation research 1976, 38 (5 Suppl 1), I31–8. [PubMed: 178460]
27. Le Page LM; Rider OJ; Lewis AJ; Noden V; Kerr M; Giles L; Ambrose LJA; Ball V; Mansor L; Heather LC; Tyler DJ, Assessing the effect of hypoxia on cardiac metabolism using hyperpolarized 13C magnetic resonance spectroscopy. NMR in Biomedicine 2019, 32 (7), e4099. [PubMed: 31090979]
28. Merritt ME; Harrison C; Storey C; Sherry AD; Malloy CR, Inhibition of carbohydrate oxidation during the first minute of reperfusion after brief ischemia: NMR detection of hyperpolarized 13CO2 and H13CO. Magnetic Resonance in Medicine 2008, 60 (5), 1029–1036. [PubMed: 18956454]
29. Clarke K; O'Connor AJ; Willis RJ, Temporal relation between energy metabolism and myocardial function during ischemia and reperfusion. Am J Physiol 1987, 253 (2 Pt 2), H412–21. [PubMed: 3618814]
30. Jin ES; Moreno KX; Wang JX; Fidelino L; Merritt ME; Sherry AD; Malloy CR, Metabolism of hyperpolarized [1-(13)C]pyruvate through alternate pathways in rat liver. NMR Biomed 2016, 29 (4), 466–74. [PubMed: 26836042]
31. Chen Y; Kim H; Bok R; Sukumar S; Mu X; Sheldon RA; Barkovich AJ; Ferriero DM; Xu D, Pyruvate to Lactate Metabolic Changes during Neurodevelopment Measured Dynamically Using Hyperpolarized 13C Imaging in Juvenile Murine Brain. Dev Neurosci 2016, 38 (1), 34–40. [PubMed: 26550989]
32. Sharma G; Wu CY; Wynn RM; Gui W; Malloy CR; Sherry AD; Chuang DT; Khemtong C, Real-time hyperpolarized (13)C magnetic resonance detects increased pyruvate oxidation in pyruvate dehydrogenase kinase 2/4-double knockout mouse livers. Sci Rep 2019, 9 (1), 16480. [PubMed: 31712597]
33. Lumata L; Yang C; Ragavan M; Carpenter N; DeBerardinis RJ; Merritt ME, Hyperpolarized (13)C Magnetic Resonance and Its Use in Metabolic Assessment of Cultured Cells and Perfused Organs. Methods Enzymol 2015, 561, 73–106. [PubMed: 26358902]
34. Nelson SJ; Kurhanewicz J; Vigneron DB; Larson PE; Harzstark AL; Ferrone M; van Criekinge M; Chang JW; Bok R; Park I; Reed G; Carvajal L; Small EJ; Munster P; Weinberg VK; Ardenkjaer-Larsen JH; Chen AP; Hurd RE; Odegardstuen LI; Robb FJ; Tropp J; Murray JA, Metabolic

imaging of patients with prostate cancer using hyperpolarized [1-(1)(3)C]pyruvate. Sci Transl Med 2013, 5 (198), 198ra108.

35. Serrao EM; Brindle KM, Potential Clinical Roles for Metabolic Imaging with Hyperpolarized [1-(13)C]Pyruvate. Front Oncol 2016, 6, 59. [PubMed: 27014634]
36. Cunningham CH; Lau JY; Chen AP; Geraghty BJ; Perks WJ; Roifman I; Wright GA; Connelly KA, Hyperpolarized 13C Metabolic MRI of the Human Heart: Initial Experience. Circ Res 2016, 119 (11), 1177–1182. [PubMed: 27635086]
37. Park Jae M; Reed Galen D; Liticker J; Putnam William C; Chandra A; Yaros K; Afzal A; MacNamara J; Raza J; Hall Ronald G; Baxter J; Derner K; Pena S; Kallem Raja R; Subramaniyan I; Edpuganti V; Harrison Crystal E; Muthukumar A; Lewis C; Reddy S; Unni N; Klemow D; Syed S; Li H; Cole S; Froehlich T; Ayers C; de Lemos J; Malloy Craig R; Haley B; Zaha Vlad G, Effect of Doxorubicin on Myocardial Bicarbonate Production From Pyruvate Dehydrogenase in Women With Breast Cancer. Circulation Research 2020, 127 (12), 1568–1570. [PubMed: 33054563]
38. Christensen CE; Karlsson M; Winther JR; Jensen PR; Lerche MH, Non-invasive in-cell determination of free cytosolic [NAD+]/[NADH] ratios using hyperpolarized glucose show large variations in metabolic phenotypes. J Biol Chem 2014, 289 (4), 2344–52. [PubMed: 24302737]
39. Park JM; Khemtong C; Liu SC; Hurd RE; Spielman DM, In vivo assessment of intracellular redox state in rat liver using hyperpolarized [1-(13) C]Alanine. Magn Reson Med 2017, 77 (5), 1741–1748. [PubMed: 28261868]
40. Spielman DM; Mayer D; Yen YF; Tropp J; Hurd RE; Pfefferbaum A, In vivo measurement of ethanol metabolism in the rat liver using magnetic resonance spectroscopy of hyperpolarized [1–13C]pyruvate. Magn Reson Med 2009, 62 (2), 307–13. [PubMed: 19526498]
41. Miller JJ; Ball DR; Lau AZ; Tyler DJ, Hyperpolarized ketone body metabolism in the rat heart. NMR Biomed 2018, 31 (6), e3912. [PubMed: 29637642]
42. Najac C; Radoul M; Le Page LM; Batsios G; Subramani E; Viswanath P; Gillespie AM; Ronen SM, In vivo investigation of hyperpolarized [1,3-(13)C2]acetoacetate as a metabolic probe in normal brain and in glioma. Sci Rep 2019, 9 (1), 3402. [PubMed: 30833594]
43. Chen W; Sharma G; Jiang W; Maptue NR; Malloy CR; Sherry AD; Khemtong C, Metabolism of hyperpolarized (13) C-acetoacetate to beta-hydroxybutyrate detects real-time mitochondrial redox state and dysfunction in heart tissue. NMR Biomed 2019, 32 (6), e4091. [PubMed: 30968985]
44. Abdurrachim D; Woo CC; Teo XQ; Chan WX; Radda GK; Lee PTH, A new hyperpolarized (13)C ketone body probe reveals an increase in acetoacetate utilization in the diabetic rat heart. Sci Rep 2019, 9 (1), 5532. [PubMed: 30940842]
45. von Morze C; Ohliger MA; Marco-Rius I; Wilson DM; Flavell RR; Pearce D; Vigneron DB; Kurhanewicz J; Wang ZJ, Direct assessment of renal mitochondrial redox state using hyperpolarized (13) C-acetoacetate. Magn Reson Med 2018, 79 (4), 1862–1869. [PubMed: 29314217]
46. Esumi K; Nishida M; Shaw D; Smith TW; Marsh JD, NADH measurements in adult rat myocytes during simulated ischemia. Am J Physiol 1991, 260 (6 Pt 2), H1743–52. [PubMed: 2058713]
47. Stoner JD; Angelos MG; Clanton TL, Myocardial contractile function during postischemic low-flow reperfusion: critical thresholds of NADH and O2 delivery. Am J Physiol Heart Circ Physiol 2004, 286 (1), H375–80. [PubMed: 12958032]
48. Opie LH; Owen P, Effects of increased mechanical work by isolated perfused rat heart during production or uptake of ketone bodies. Assessment of mitochondrial oxidized to reduced free nicotinamide-adenine dinucleotide ratios and oxaloacetate concentrations. Biochem J 1975, 148 (3), 403–15. [PubMed: 173281]
49. Opie LH; Owen P; Thomas M; Samson R, Coronary sinus lactate measurements in assessment of myocardial ischemia. Comparison with changes in lactate-pyruvate and beta-hydroxybutyrate-acetoacetate ratios and with release of hydrogen, phosphate and potassium ions from the heart. Am J Cardiol 1973, 32 (3), 295–305. [PubMed: 4725585]
50. Hou WL; Yin J; Alimujiang M; Yu XY; Ai LG; Bao YQ; Liu F; Jia WP, Inhibition of mitochondrial complex I improves glucose metabolism independently of AMPK activation. J Cell Mol Med 2018, 22 (2), 1316–1328. [PubMed: 29106036]

51. Kuznetsov AV; Winkler K; Kirches E; Lins H; Feistner H; Kunz WS, Application of inhibitor titrations for the detection of oxidative phosphorylation defects in saponin-skinned muscle fibers of patients with mitochondrial diseases. Biochimica et Biophysica Acta (BBA) - Molecular Basis of Disease 1997, 1360 (2), 142–150. [PubMed: 9128179]
52. Barron JT; Gu L; Parrillo JE, Malate-aspartate shuttle, cytoplasmic NADH redox potential, and energetics in vascular smooth muscle. J Mol Cell Cardiol 1998, 30 (8), 1571–9. [PubMed: 9737943]
53. Barron JT; Gu L; Parrillo JE, NADH/NAD redox state of cytoplasmic glycolytic compartments in vascular smooth muscle. Am J Physiol Heart Circ Physiol 2000, 279 (6), H2872–8. [PubMed: 11087243]
54. Xiao W; Loscalzo J, Metabolic Responses to Reductive Stress. Antioxid Redox Signal 2020, 32 (18), 1330–1347. [PubMed: 31218894]
55. Hwang YC; Kaneko M; Bakr S; Liao H; Lu Y; Lewis ER; Yan S; Ii S; Itakura M; Rui L; Skopicki H; Homma S; Schmidt AM; Oates PJ; Szabolcs M; Ramasamy R, Central role for aldose reductase pathway in myocardial ischemic injury. FASEB J 2004, 18 (11), 1192–9. [PubMed: 15284219]
56. Ramasamy R; Trueblood N; Schaefer S, Metabolic effects of aldose reductase inhibition during low-flow ischemia and reperfusion. Am J Physiol 1998, 275 (1), H195–203. [PubMed: 9688914]
57. Haworth RA; Berkoff HA, The control of sugar uptake by metabolic demand in isolated adult rat heart cells. Circ Res 1986, 58 (1), 157–65. [PubMed: 3510759]
58. White RL; Wittenberg BA, NADH fluorescence of isolated ventricular myocytes: effects of pacing, myoglobin, and oxygen supply. Biophys J 1993, 65 (1), 196–204. [PubMed: 8369428]
59. Bunger R, Compartmented pyruvate in perfused working heart. Am J Physiol 1985, 249 (3 Pt 2), H439–49. [PubMed: 2994495]
60. Day SE; Kettunen MI; Gallagher FA; Hu DE; Lerche M; Wolber J; Golman K; Ardenkjaer-Larsen JH; Brindle KM, Detecting tumor response to treatment using hyperpolarized 13C magnetic resonance imaging and spectroscopy. Nat Med 2007, 13 (11), 1382–7. [PubMed: 17965722]
61. Khemtong C; Carpenter NR; Lumata LL; Merritt ME; Moreno KX; Kovacs Z; Malloy CR; Sherry AD, Hyperpolarized 13C NMR detects rapid drug-induced changes in cardiac metabolism. Magn Reson Med 2015, 74 (2), 312–9. [PubMed: 25168480]
62. Cohen MS, Interplay between compartmentalized NAD(+) synthesis and consumption: a focus on the PARP family. Genes Dev 2020, 34 (5–6), 254–262. [PubMed: 32029457]
63. Stride N; Larsen S; Hey-Mogensen M; Sander K; Lund JT; Gustafsson F; Kober L; Dela F, Decreased mitochondrial oxidative phosphorylation capacity in the human heart with left ventricular systolic dysfunction. Eur J Heart Fail 2013, 15 (2), 150–7. [PubMed: 23115323]
64. Halestrap AP, The monocarboxylate transporter family--Structure and functional characterization. IUBMB Life 2012, 64 (1), 1–9. [PubMed: 22131303]
65. Harris T; Eliyahu G; Frydman L; Degani H, Kinetics of hyperpolarized 13C1-pyruvate transport and metabolism in living human breast cancer cells. Proc Natl Acad Sci U S A 2009, 106 (43), 18131–6. [PubMed: 19826085]
66. Rao Y; Gammon S; Zacharias NM; Liu T; Salzillo T; Xi Y; Wang J; Bhattacharya P; Piwnica-Worms D, Hyperpolarized [1-(13)C]pyruvate-to-[1-(13)C]lactate conversion is rate-limited by monocarboxylate transporter-1 in the plasma membrane. Proc Natl Acad Sci U S A 2020, 117 (36), 22378–22389. [PubMed: 32839325]
67. Moon RB; Richards JH, Determination of intracellular pH by 31P magnetic resonance. J Biol Chem 1973, 248 (20), 7276–8. [PubMed: 4743524]
68. Bottomley PA; Hardy CJ; Weiss RG, Correcting human heart 31P NMR spectra for partial saturation. Evidence that saturation factors for PCr/ATP are homogeneous in normal and disease states. Journal of Magnetic Resonance (1969) 1991, 95 (2), 341–355.
69. Spencer RG; Balschi JA; Leigh JS Jr.; Ingwall JS, ATP synthesis and degradation rates in the perfused rat heart. 31P-nuclear magnetic resonance double saturation transfer measurements. Biophys J 1988, 54 (5), 921–9. [PubMed: 3242635]

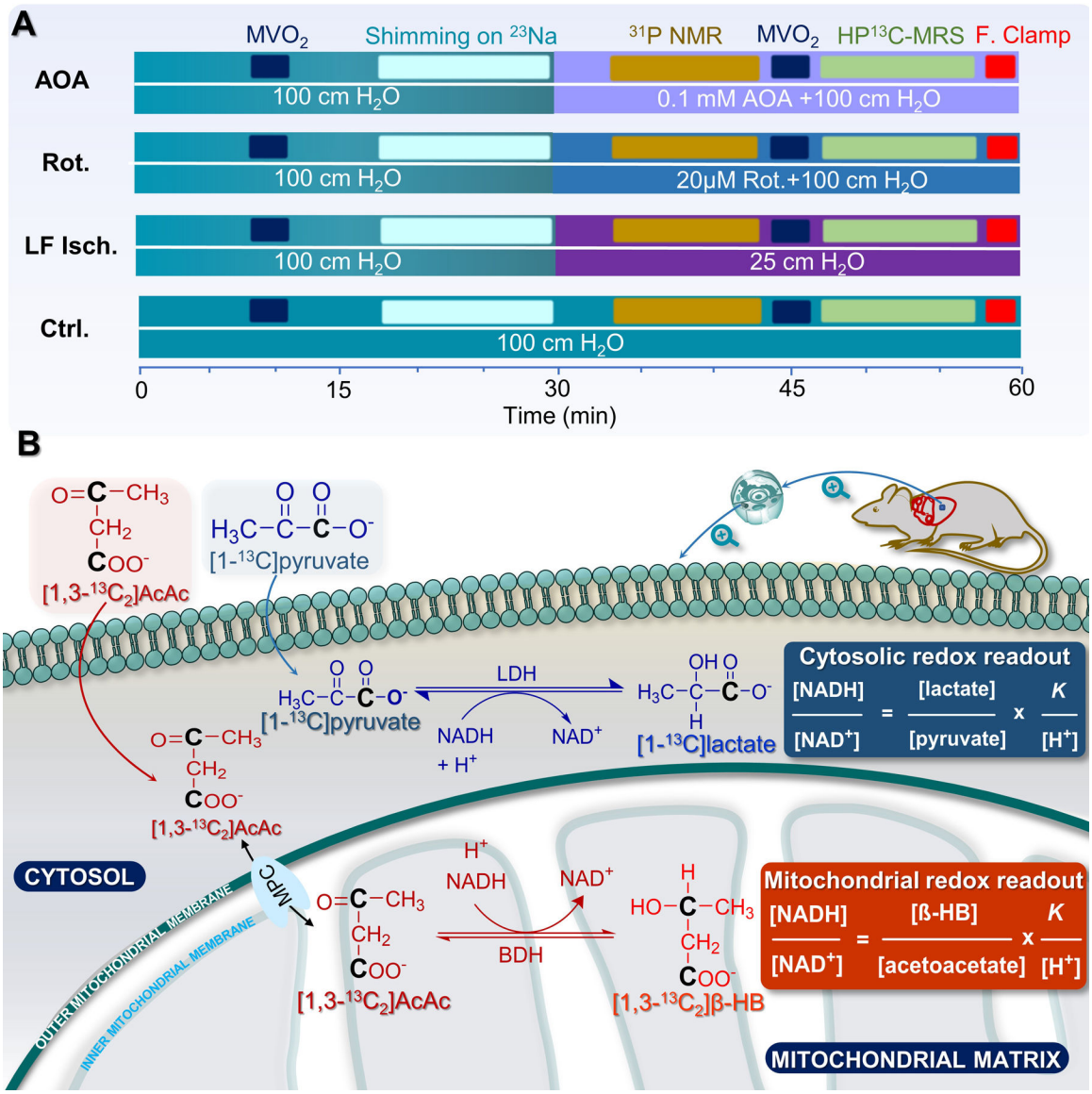

Figure 1.

(A) A diagram showing the perfusion timeline for all groups of hearts; and (B) a scheme illustrating the metabolism of [1-^{13}C]pyruvate to [1-^{13}C]lactate and [1,3-$^{13}C_2$]AcAc to [1,3-$^{13}C_2$]β-hydroxybutyrate in the cytosolic and mitochondrial compartments, respectively.

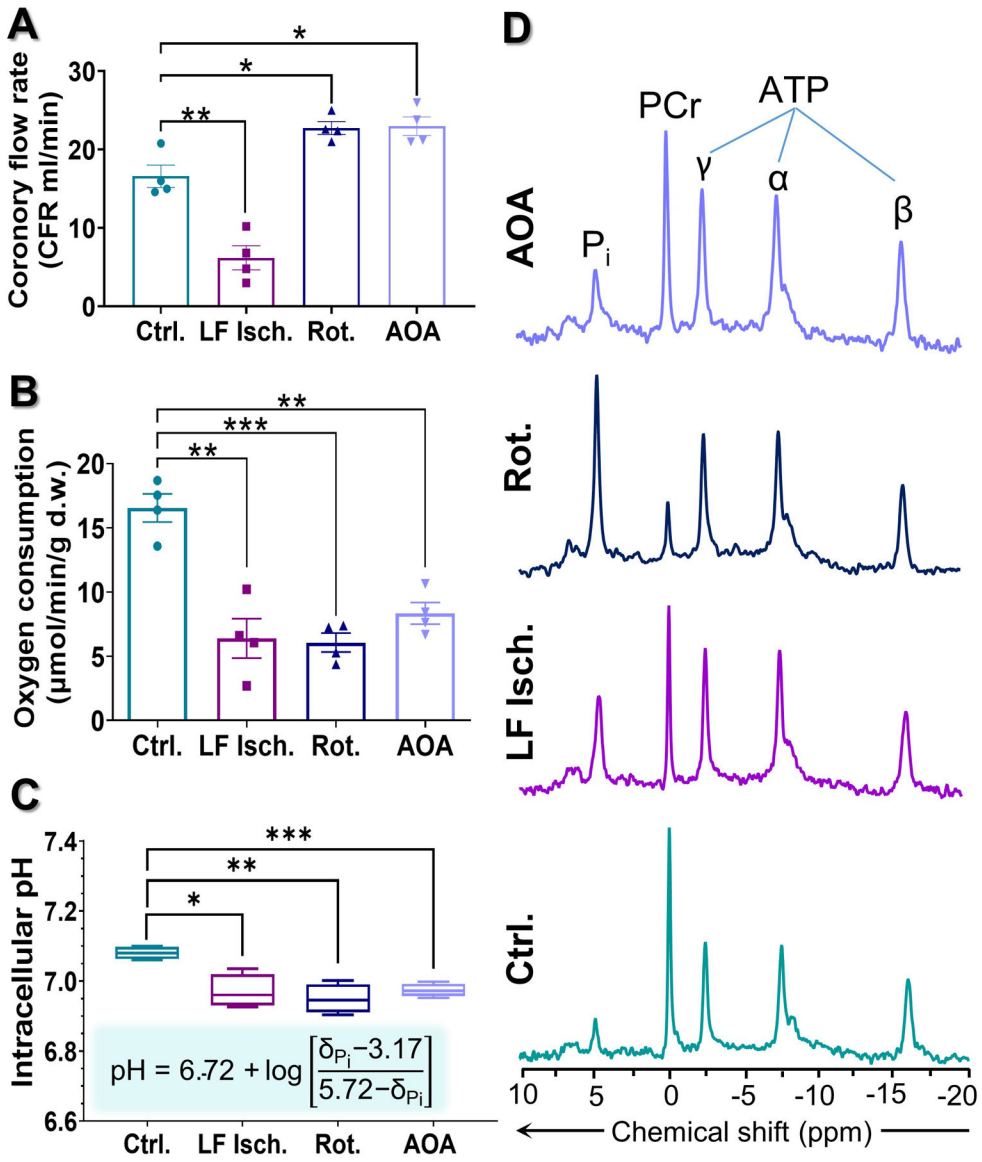

Figure 2.

Plots indicating (**A**) coronary flow rate, (**B**) myocardial oxygen consumption, and (**C**) intracellular pH of the hearts during perfusion. (**D**) ^{31}P NMR spectrum of control, low-flow ischemia, rotenone-treated, or AOA-treated perfused heart. Intracellular pH values were calculated using the modified Henderson–Hasselbalch equation from the chemical shift of inorganic phosphate (P_i) ^{31}P resonances. Data are shown as the mean ± SEM (n= 4) with statistical significance of differences indicated by "*" ($P < 0.05$), "**" ($P < 0.001$), and "***" ($P < 0.0001$).

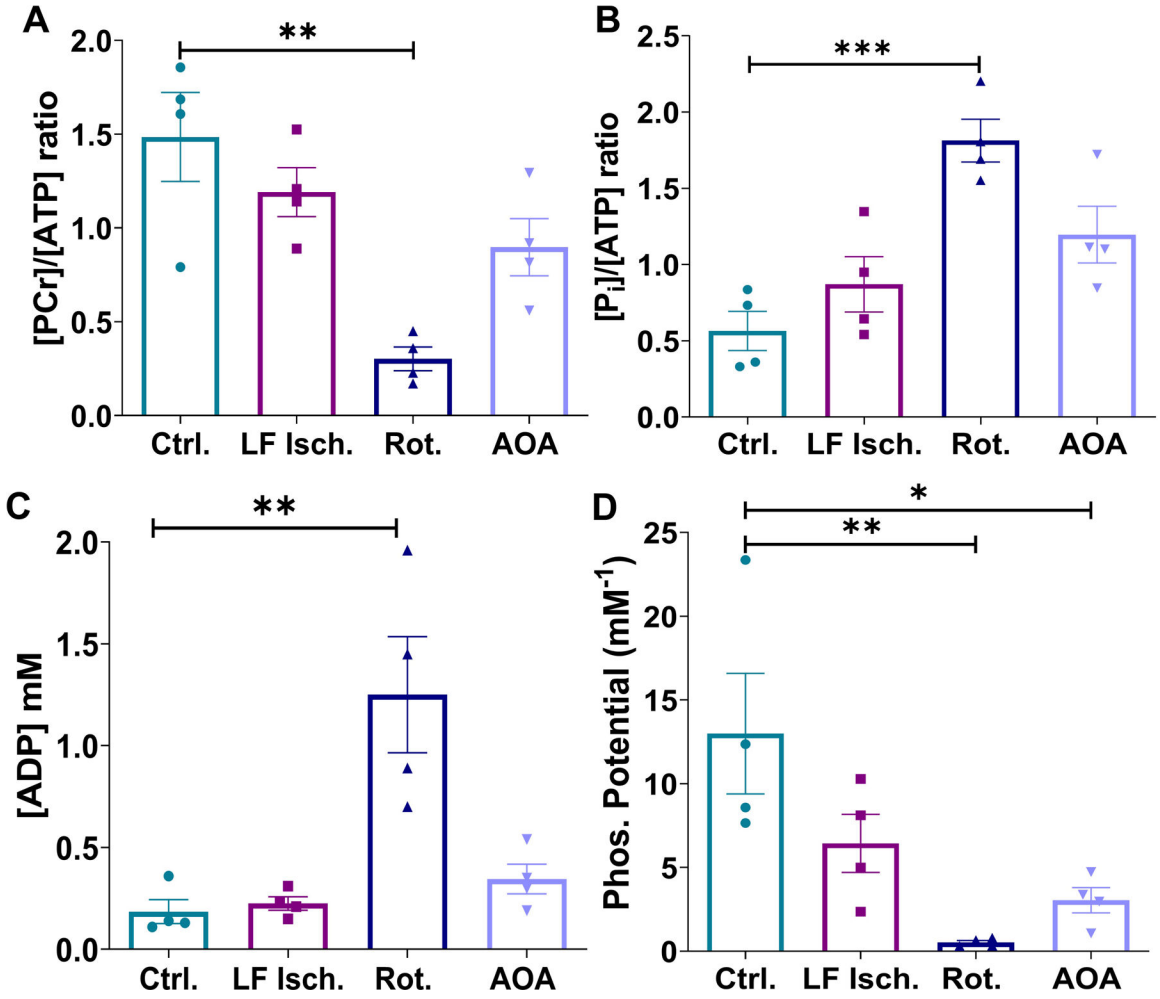

Figure 3.

Bar graphs showing phosphocreatine to ATP ratio (**A**), inorganic phosphate to ATP ratio (**B**), estimated ADP concentration (**C**), and phosphorylation potential (**D**) of all four groups of perfused hearts. The metabolite ratios were calculated from ^{31}P NMR signal intensities, corrected for T_1 decay, according to previously published methods [68, 69]. [ADP] and phosphorylation potential were calculated using methods previously reported by Clarke et al.[29]. Data are shown as the mean ± SEM (n= 4) with statistical significance of differences indicated by "*" ($P < 0.05$), "**" ($P < 0.001$), and "***" ($P < 0.0001$).

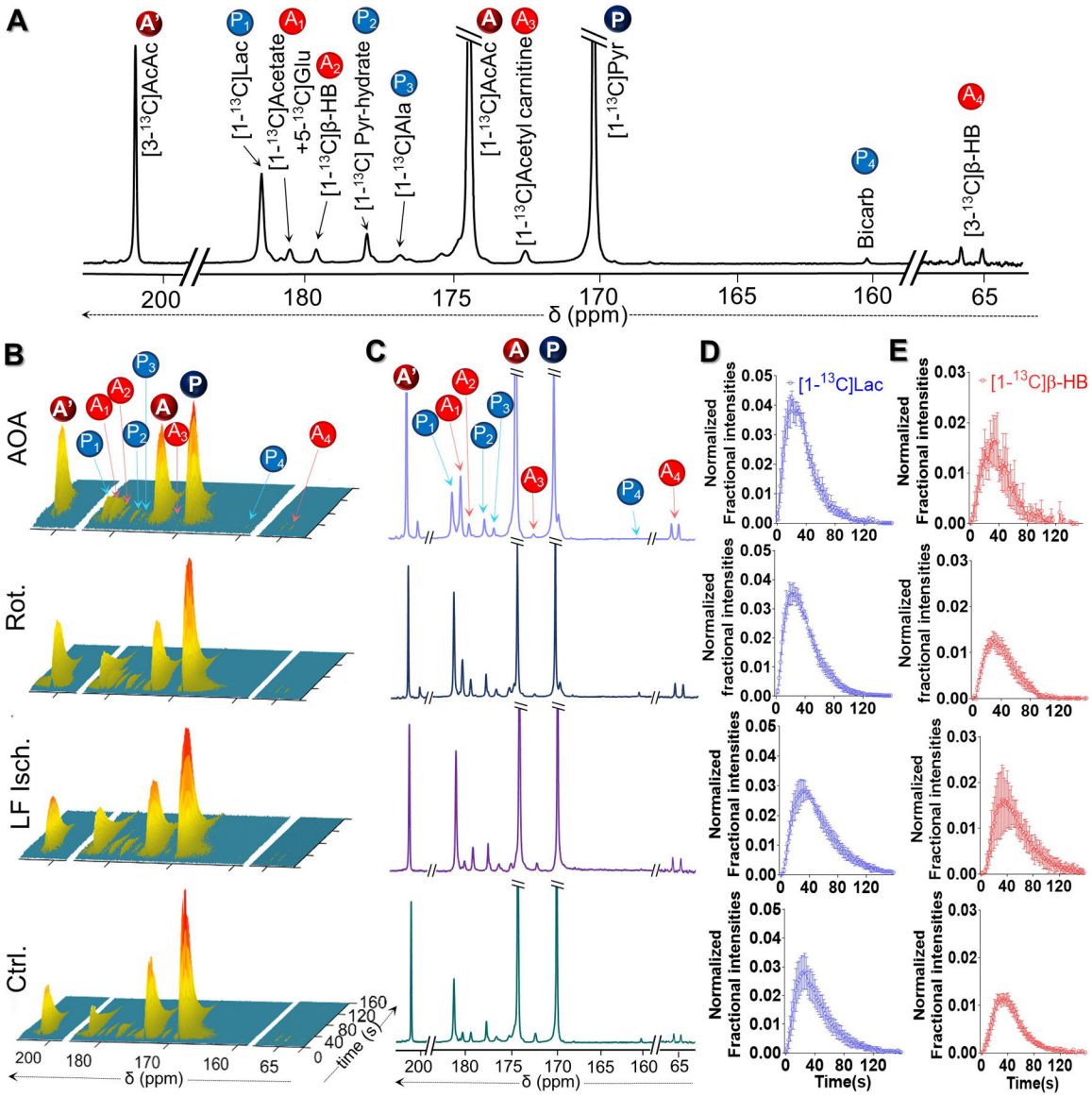

Figure 4.

(**A**) Representative ^{13}C NMR spectra of a perfused rat heart injected with co-polarized [1-^{13}C]pyruvate and [1,3-$^{13}C_2$]AcAc, showing resonances of [1-^{13}C]pyruvate (P), [1,3-$^{13}C_2$]AcAc (A and A´), and their downstream metabolites. P_1-P_4 = metabolic products of [1-^{13}C]pyruvate; A_1-A_4 = metabolic products of [1,3-$^{13}C_2$]AcAc. (**B**) Representative sequential ^{13}C NMR spectra, displayed as stacked plots, of the perfused hearts following the injection of co-polarized [1-^{13}C]pyruvate and [1,3-$^{13}C_2$]AcAc. Each spectrum was acquired every 2 s. Corresponding summed spectra of these arrays are shown in panel (**C**). Averaged normalized signal intensities (4 hearts per group) of HP [1-^{13}C]lactate and C-1 of HP [1,3-$^{13}C_2$]β-HB plotted as a function of perfusion time are shown in panels (**D**) and (**E**), respectively. At a given time point, the HP [1-^{13}C]lactate signal was normalized to the total HP ^{13}C signals of downstream metabolites originated from HP [1-^{13}C]pyruvate summed over the NMR acquisition time window for each heart, ~150 s. Meanwhile, the HP [1-^{13}C]β-

HB signal was normalized to the total metabolites originated from HP [1,3-$^{13}C_2$]AcAc during the same time window.

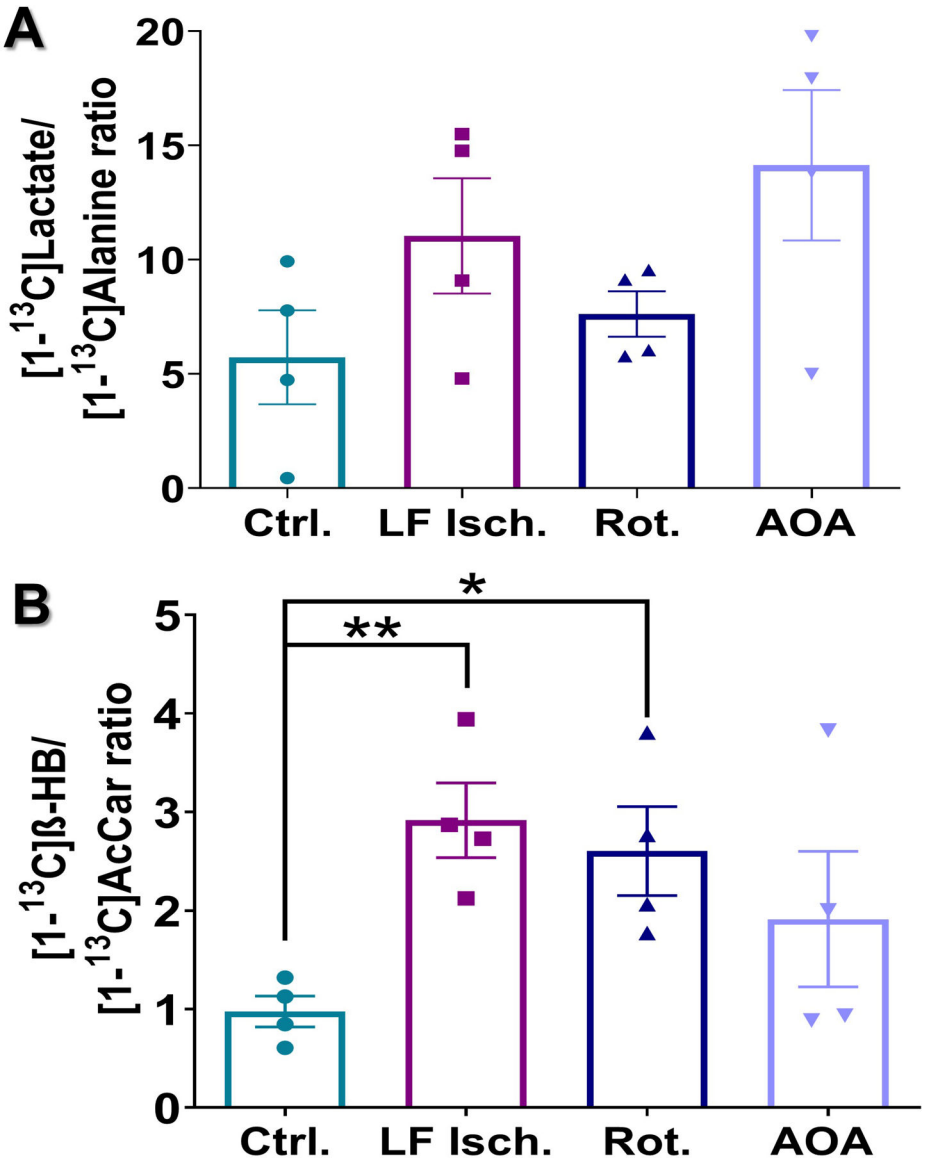

Figure 5.

Production of HP [1-^{13}C]lactate (**A**) and HP [1-^{13}C]β-HB (**B**) in the hearts following the injection of co-polarized [1-^{13}C]pyruvate and [1,3-$^{13}C_2$]AcAc. Intensities of HP [1-^{13}C]lactate were normalized to HP [1-^{13}C]alanine produced by the same heart. HP [1-^{13}C]β-HB intensities were normalized to HP [1-^{13}C]acetyl-carnitine. Data are presented as the mean ± SEM (n = 4 per group) with statistical significance of differences indicated by "*" ($P < 0.05$) and "**" ($P < 0.001$).

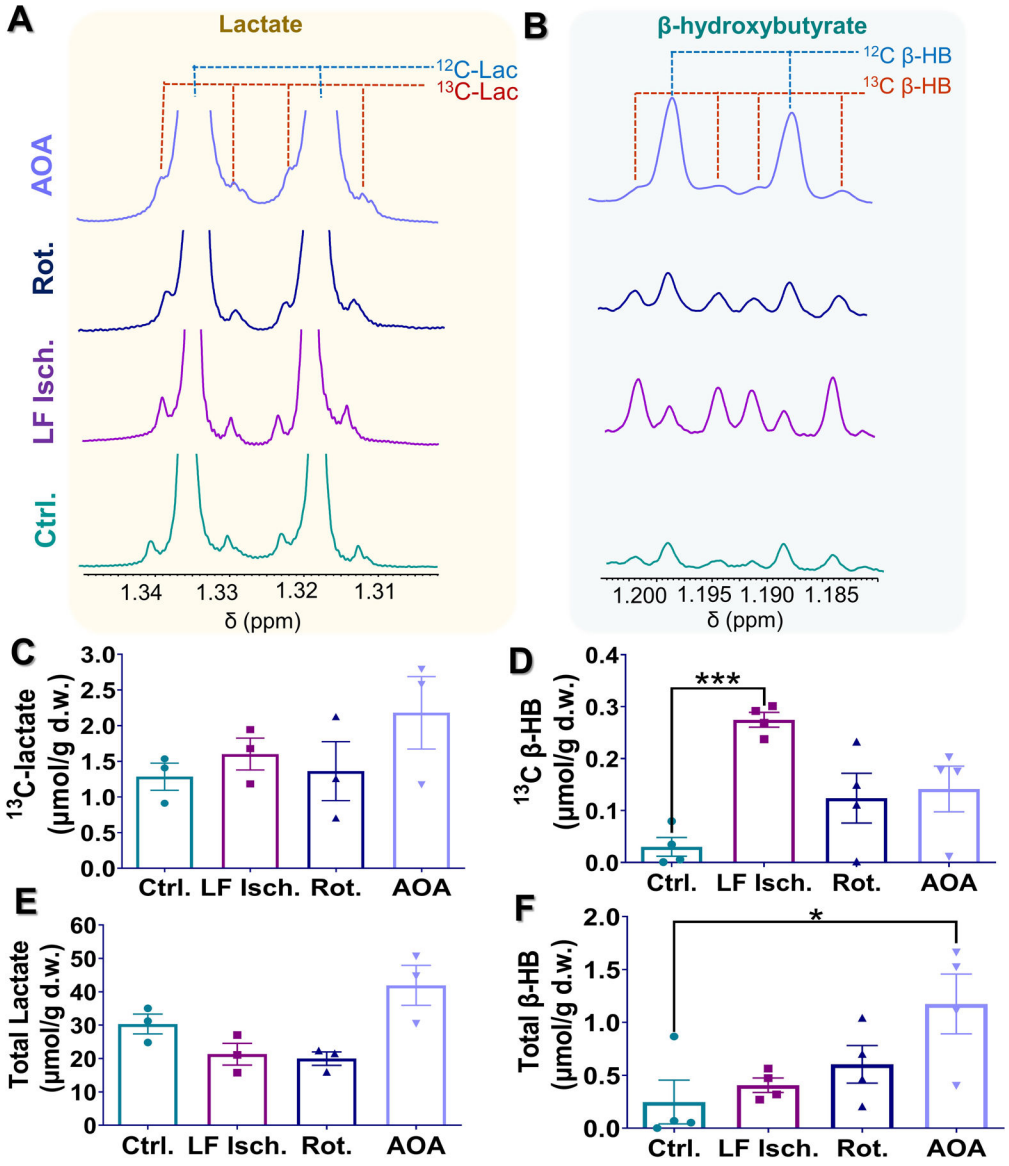

Figure 6.

(**A-B**) Representative high-resolution ^{1}H NMR spectra of tissue extracts of hearts perfused under different conditions. For each spectrum, methyl resonances of lactate and β-hydroxybutyrate are shown. (**C-F)** Average tissue lactate and β-hydroxybutyrate concentrations quantified from the ^{1}H NMR spectra are shown in. Tissue concentrations are shown as the mean ± SEM (n = 4) with statistical significance of differences indicated by "*" ($P < 0.05$) and "***" ($P < 0.0001$).